Inorganic Chemistry

Article

pubs.acs.org/IC

Two High-Pressure Phases of SiS_2 as Missing Links between the Extremes of Only Edge-Sharing and Only Corner-Sharing Tetrahedra

Jürgen Evers,* Peter Mayer, Leonhard Möckl, and Gilbert Oehlinger

Department of Chemistry, Ludwig-Maximilian University of Munich, Butenandtstr. 5-13, D-81377 Munich, Germany

Ralf Köppe and Hansgeorg Schnöckel*

Karlsruher Institut für Technologie (KIT), Institut für Anorganische Chemie, Engesserstr.15, Gebäude 30.45, D-76131 Karlsruhe, Germany

Supporting Information

ABSTRACT: The ambient pressure phase of silicon disulfide (NP-SiS_2), published in 1935, is orthorhombic and contains chains of distorted, edge-sharing SiS_4 tetrahedra. The first high pressure phase, HP3-SiS_2, published in 1965 and quenchable to ambient conditions, is tetragonal and contains distorted corner-sharing SiS_4 tetrahedra. Here, we report on the crystal structures of two monoclinic phases, HP1-SiS_2 and HP2-SiS_2, which can be considered as missing links between the orthorhombic and the tetragonal phase. Both monoclinic phases contain edge- as well as corner-sharing SiS_4 tetrahedra. With increasing pressure, the volume contraction $(-\Delta V/V)$ and the density, compared to the orthorhombic NP-phase, increase from only edge-sharing tetrahedra to only corner-sharing tetrahedra. The lattice and the positional parameters of NP-SiS_2, HP1-SiS_2, HP2-SiS_2, and HP3-SiS_2 were derived in good agreement with the experimental data from group−subgroup relationships with the CaF_2 structure as aristotype. In addition, the Raman spectra of SiS_2 show that the most intense bands of the new phases HP1-SiS_2 and HP2-SiS_2 (408 and 404 cm^{-1}, respectively) lie between those of NP-SiS_2 (434 cm^{-1}) and HP3-SiS_2 (324 cm^{-1}). Density functional theory (DFT) calculations confirm these observations.

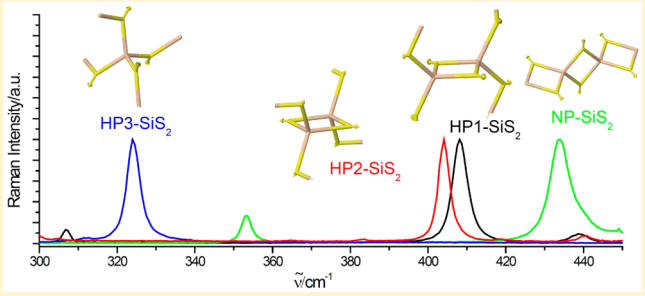

1. INTRODUCTION

New binary compounds and new modifications, as well as new isomers of molecular species of two main group elements (especially if light and frequently appearing elements of the Earth's crust are involved) are of fundamental interest, since basic conclusions regarding bonding and geometric structure for chemistry in general can be drawn. Against this background, silicon sulfur compounds or molecular species play a prominent role: In the molecular area, the detection of the CO_2 and SiO_2 analogue S═Si═S species was a highlight. Gaseous SiO_2 and also SiS_2 cannot be obtained via the vaporization of the solid compounds, because, e.g., the decomposition of SiO_2 to $SiO(g)$ and O_2 ($SiS(g) + {}^1/_2S_2$) is thermodynamically favored. Both molecular species O═Si═O and S═Si═S possess a similar electronic ground states and are of linear shape (symmetry $D_{\infty h}$). They are formed in solid rare-gas matrices[1] at 10 K via chemical reactions of either molecular SiO with O atoms obtained in a glow discharge or molecular SiS with S atoms formed after photochemical dissociation of COS to S atoms and CO.[1] Very recently, an excited isomer of SiS_2 (76 kJ/mol above the linear ground state) also has been structurally characterized by high-resolution rotational spectroscopy under discharge.[2] This bent SiS_2 molecule of symmetry C_{2v} may theoretically represent a building block for the linear chainlike ambient pressure (NP) SiS_2 modification (cf. discussion below).

However, in this article, we concentrate on the solid-state phases and, therefore, in this Introduction, will start with the two most abundant elements—silicon and oxygen—and their famous binary compound silica (SiO_2). It plays an important role in the interior of the Earth and is also of great technological interest.[3] At NP, it provides examples of first-order reconstructive and of soft-mode-driven displacive transitions and, at high pressure (HP), examples of pressure-induced polymorphism and also amorphization. At ambient pressure, SiO_2 crystallizes with a silicon coordination number of 4, similar to that of quartz, tridymite, and cristobalite, each existing with low- and high-temperature forms.[4] Since the discovery of its HP polymorphism to stishovite (rutile structure, silicon coordination number of 6),[5] molecular dynamics (MD) predicted HP phases with higher density, ranging from 4.01 g cm^{-3} (α-PbO_2 structure, silicon coordination number of 6) to 4.24 g cm^{-3} (CaF_2 structure, silicon coordination number of 8).[6] However, up to this point in time, SiO_2 with CaF_2 structure has not been

Received: July 28, 2014
Published: January 15, 2015

DOI: 10.1021/ic501825r
Inorg. Chem. 2015, 54, 1240−1253

experimentally confirmed, but a high-pressure phase with a pyrite structure (silicon coordination number of 6 + 2) above 102 GPa and 2400 K[7] was obtained in diamond anvil cell experiments. Density functional theory (DFT) calculations predict SiO_2 with a Fe_2P structure (silicon coordination number of 9)[8] at ultrahigh pressures of 1.04 TPa, possibly stable in exoplanets, which have a mass up to 10 times greater than that of the Earth.

Although SiS_2 is iso-valence electronic to SiO_2, its structural diversity is smaller. At the start of our investigations, only two SiS_2 phases had been characterized by single-crystal structure analysis. In 1935, Zintl and Loosen[9] and Büssem et al.[10] both investigated NP-SiS_2. It crystallizes in an orthorhombic structure (*oI*12, *Ibam*, $Z = 4$) with chains of distorted edge-sharing tetrahedra running parallel to the *c*-axis. Almost 50 years later, Peters and Krebs refined this structure and also that of isotypic $SiSe_2$[11] with modern diffractometric techniques at 138 K and at 293 K.[12] In addition, beryllium dihalogenides BeX_2 (X = Cl, Br, I) have also been established with the orthorhombic SiS_2 structure.[13]

The first HP experiments on SiS_2 were submitted by Silverman and Soulen in August 1964 and published in 1965.[14] They used a tetrahedral anvil press in the pressure range of 2.5−8.0 GPa and in the temperature range of $T = 973$−2573 K and prepared three different microcrystalline phases, which could be quenched to ambient conditions. Derived from powder X-ray patterns, lists of *d*-values were published, along with the intensities of these phases. One pattern was indexable with a tetragonal lattice ($a = 5.43$, $c = 8.67$ Å),[14] but no structural information about these HP phases was obtained until June 1965. Then, Prewitt and Young[15] also used a tetrahedral anvil press for HP experiments with SiS_2 and GeS_2 (6.0−6.5 GPa, $T = 1148$−1573 K) and prepared tetragonal single crystals (SiS_2: $a = 5.420(4)$ Å, $c = 8.718(4)$ Å; GeS_2: $a = 5.480(4)$ Å, $c = 9.143(4)$ Å). Indeed, for tetragonal SiS_2, they synthesized the same HP phase as that reported by Silverman and Soulen.[14] Here, this phase is called HP3-SiS_2. By single-crystal investigations, HP3-SiS_2 and HP-GeS_2 were found to be isotypic. They crystallize in the space group $I\bar{4}2d$ with a new structure type. Slightly distorted SiS_4 tetrahedra share all corners and form a three-dimensional net. The density (ρ) increases from 2.052 g cm^{-3} for the orthorhombic NP phase to 2.391 g cm^{-3} for the tetragonal HP3-phase, which corresponds to an increase in $\Delta\rho/\rho$ of 14.2%. At ambient pressure, this structure is also stable in α-$ZnCl_2$.[16]

In 1991, Guseva et al.[17] also performed HP experiments on SiS_2 (2.5−6.0 GPa, $T = 1273$−1473 K). They observed different HP phases and published lists of *d*-values with intensities, derived from powder X-ray patterns. Two lists were almost identical with those published by Silverman and Soulen[14] nearly 30 years earlier, but two of them had not been observed earlier. Because of the poor quality of their powder X-ray patterns, it was not possible to derive structural data for these two new HP phases.

It was our intention to perform structural investigations on SiS_2, both at NP and at HP, and to search for phases with negative thermal expansion (NTE),[18−20] which are of great technological interest. Recently, we derived NTE phases for tetramorphic palladium(II) chloride.[21] Interestingly, in 1938, Wells[22] was the first to give a hint to the structural relation between α-$PdCl_2$ and the orthorhombic phase of NP-SiS_2.[22] In the α-, γ-, and δ-polymorphs of $PdCl_2$, slightly distorted $PdCl_4$ squares are found that share edges (α, δ) and corners (γ). These three $PdCl_2$ phases exhibit up to 873 K (γ) and 1173 K (α, δ) NTE effects in directions with edge-sharing. In both compounds, AB_4 polyhedra share edges: the first with $PdCl_4$ squares, the last with SiS_4 tetrahedra. Therefore, the question arises if in SiS_2 with chains of edge-connected polyhedra the NTE effect, or at least uncommon small thermal expansion, is observed.

In this investigation, we report on the structural solution of the two HP phases of SiS_2, which were first prepared by Guseva et al.[17] The structural data were derived by single-crystal X-ray investigations (NP and HP3 phases). In addition, thermal expansion was investigated by single-crystal determination on the orthorhombic NP phase and also on the tetragonal HP3-SiS_2 phase. For the two new HP1-SiS_2 and HP2-SiS_2 phases, heating experiments were performed on an X-ray Guinier diffractometer up to ∼700 K. The Raman spectra of tetramorphic SiS_2 were recorded and discussed, with respect to their structural motifs.

To complete the exciting field of solid MS_2 phases, the published work on GeS_2 with its low-temperature (LT) modification[23] (density $\rho_{calc} = 2.99$ g cm^{-3}) and its high-temperature (HT) modification[24] ($\rho_{calc} = 2.935$ g cm^{-3}) should be mentioned. In the LT phase, chains of GeS_4 tetrahedra are found where each tetrahedron shares two corners with other tetrahedra and two corners remain uncoordinated, forming a three-dimensional (3D) net. In HT-GeS_2, double tetrahedra build up a layer structure in which only one edge is shared. From the remaining four corners, two are shared, and the other two remain uncoordinated. In addition, in 1973, Wang and Horn[25] used hydrothermal synthesis at 0.1 GPa and 1113 K to prepare a microcrystalline tetragonal GeS_2 phase with space group $I4_1/acd$, but could not deduce the structure. In 1998, Manners et al.[26] solved this structure: δ-GeS_2 contains assemblies of adamantanoid Ge_4S_{10} secondary building blocks ($\rho_{calc} = 3.17$ g cm^{-3}). However, the earlier-mentioned HP phase of GeS_2 shows a density of $\rho_{calc} = 3.31$ g cm^{-3}, which is the highest density for tetramorphic GeS_2. A Diamond2 view[27] with the crystal structures of GeS_2 is shown in Figures S1−S4 in the Supporting Information (SI).

2. RESULTS AND DISCUSSION

Orthorhombic NP-SiS_2. The orthorhombic NP-SiS_2 phase[9,10,12] contains chains of distorted edge-sharing SiS_4 tetrahedra along the *c*-axis. One can expect very rigid bonding between the tetrahedra in this direction. Therefore, single-crystal X-ray reinvestigations, including determination of thermal expansion, were performed on NP-SiS_2. The results are summarized in Table S1 in the SI.

The lattice, the positional, and the thermal parameters of NP-SiS_2 in this investigation at 103(2) K and at 300(2) K deviate only slightly from the results of the earlier investigation by Peters and Krebs in 1982;[12] one should keep in mind that the measuring temperatures of Peters and Krebs[12] (138, 293 K) differ from those in our experiments (103, 300 K).

Figure 1a shows Guinier diffractograms (Mo $K\alpha_1$ radiation) of NP-SiS_2 from 6° to 46° (2θ) and at $T = 300(2)$−707(5) K; Figure 1b shows the relative change (%) of the lattice parameters *a*, *b*, and *c* and the cell volume (*V*) at various temperatures. In Figures 1c and 1d, Diamond2 views[27] are presented of NP-SiS_2 at 300(2) K along the [010] and [001] axes with anisotropic displacement spheres of 50% probability. In Figure 1e, distances (Å) and angles (deg) for orthorhombic NP-SiS_2 at 300 K are summarized.

DOI: 10.1021/ic501825r
Inorg. Chem. 2015, 54, 1240−1253

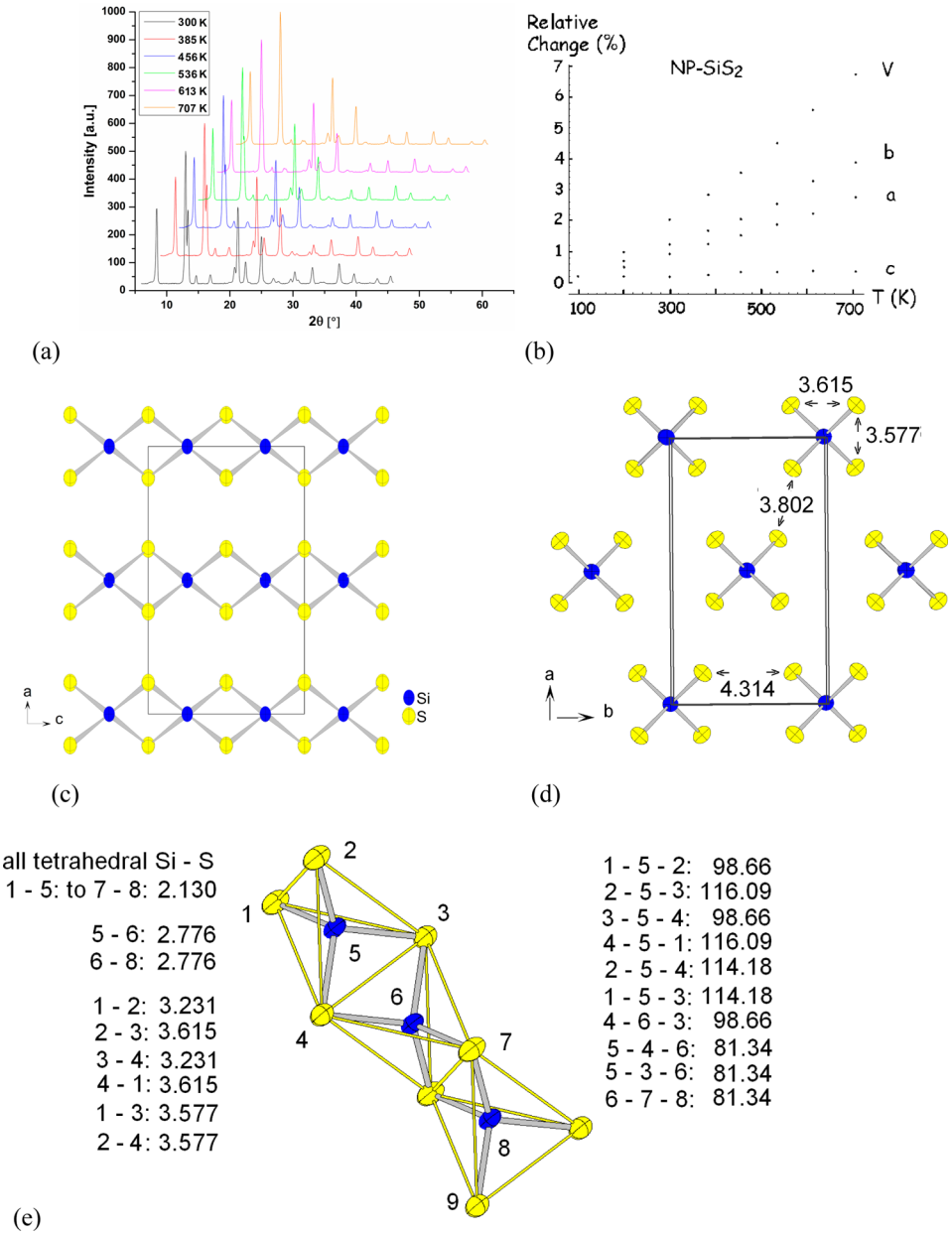

Figure 1. (a) Guinier diffractograms (Mo Kα_1 radiation) of NP-SiS_2 from 6° to 46° (2θ) with an increment of 0.04° and a counting time of 10 s per increment (T = 300(2)−707(5) K). (b) Relative change (%) of the lattice parameters a, b, and c and the cell volume (V) at various temperatures. The data between 103(2) K and 385(2) K were obtained by single-crystal X-ray analysis (Table S1 in the SI), those up to 707(5) K by Guinier powder X-ray investigations. (In the investigated temperature range, NP-SiS_2 shows no clear negative thermal expansion (NTE). The thermal expansion of parameter c is the lowest, but with the exception between 100(2) K and 200(2) K (Table S1 in the SI), it is slightly positive; the expansion of a, b, and V is positive.) (c) Diamond2 view[27] of NP-SiS_2 at 300(2) K along the [010] axis with anisotropic displacement ellipsoids of 50% probability: edge-sharing of distorted tetrahedra in the c-direction. (d) View along the c-axis with one-dimensional interbonding of SiS_4 tetrahedra. (The S−S-distances (given in Ångstroms) within and between the tetrahedra are summarized in order to show the "open" structure in the other two directions (a and in b), where only weak van der Waals bonding between the tetrahedra is present.) (e) Distances (Å) and angles (deg) (experimental errors of ±0.002 Å and ±0.02°, respectively) summarized for orthorhombic NP-SiS_2 at 300 K (Table S1 in the SI).

Figure 1b shows that bonding in the c-direction is the strongest for the highly anisotropic structure. Here, the thermal expansion is the lowest (see Table S1 in the SI). With the exception between 103(2) K and 200(2) K, it is slightly positive. Also, the U_{33} displacement parameters ($U_{33,Si}$ = 0.0100(3) Å^2, $U_{33,S}$ = 0.0119(3) Å^2 (at 103(2) K; see Table S1 in the SI)) are the smallest, in comparison with U_{11} and U_{22}. Therefore, the ellipsoids in the c-direction are smaller than in the a- and b-directions. As already mentioned, α-$PdCl_2$ with edge-sharing $PdCl_4$ squares[21] shows a negative NTE in the c-direction. However, the U_{33} displacement parameters of α-$PdCl_2$ at 100(2) K ($U_{33,Pd}$ = 0.0063(2), $U_{33,Cl}$ = 0.0086(4) Å^2)[21] show much smaller values than those of NP-SiS_2 at 100(2) K, indicating stronger bonding in the c-direction for α-$PdCl_2$.

The Si−S distances at 300(2) K in the distorted tetrahedra (Figure 1e) are 2.130(2) Å, and the S−S distances are between 3.231(2) Å and 3.615(2) Å. The sharing of edges leads to planar Si_2S_2 rings (4−5−3−6). The sum of the angles is 360.0° (81.34° (2×), 98.66° (2×)). The other angles for the distorted tetrahedra are 114.18° and 116.09°. For the edge-sharing of

DOI: 10.1021/ic501825r
Inorg. Chem. 2015, 54, 1240−1253

SiS_4, the tops of the tetrahedra are in "anti" position (Figure 1e, S(2) atom up, S(9) atom down).

The density of orthorhombic NP-SiS_2[9,10,12] (ρ_{calc} = 2.044(2) g cm^{-3}, 300(2) K; see Table S1 in the SI) is the lowest of all four phases. The one-dimensional chains are built up by interbonded tetrahedra in the *c*-direction. Therefore, they are not very efficiently packed in the *a*- and *b*-directions via only weak van der Waals interaction between them. The distances between the chains are 3.802(5) and 4.314(5) Å (Figure 1d). Therefore, one could think about high-pressure–high-temperature transformations from this "open", one-dimensional arrangement of distorted SiS_4 tetrahedra of chains to a "closer", two-dimensional arrangement in layers and, finally, to a three-dimensional one in a network in order to lower the van der Waals space and increase the density.

Monoclinic HP1-SiS_2 and HP2-SiS_2. During our investigations on SiS_2 in the high-pressure high-temperature field, Guinier diffractograms of two phases were obtained, neither indexable with the orthorhombic NP[9,10,12] nor with the earlier-known tetragonal HP phase.[14,15] The published *d*-values and intensities for the new HP phases published in 1991 by Guseva et al.[17] are in agreement with our indexing. Both new phases—here, called HP1-SiS_2 and HP2-SiS_2, numbered according to increasing pressure—are monoclinic and could be indexed with high reliability indices (see Experimental Details). Comparison of the unit-cell volumes (V_{HP1} = 273.42, V_{HP2} = 784.10 Å^3 (cf. below)) with those of the orthorhombic NP-SiS_2 phase (V_{NP} = 299.66(2) Å^3) and of the tetragonal HP3-SiS_2 phase (V_{HP3} = 256.10(5) Å^3) shows that the HP1 phase contains four formula units as the NP and HP3 phases. For HP2-SiS_2, the unit-cell volume is tripled ($V_{HP2}/3$ = 784.10/3 Å^3 = 261.37 Å^3) which results in 12 formula units. By cooling the belt apparatus slowly from 1473 K to room temperature within 8 h, at 2.8 GPa for HP1-SiS_2 and 3.5 GPa for HP2-SiS_2, single crystals were obtained (however, in both cases, without well-developed faces). Nevertheless, they were suitable for single-crystal investigations. The crystallographic data for monoclinic HP1-SiS_2 and HP2-SiS_2 are summarized in Tables S2 and S3 in the SI.

Hence, up to 6 GPa and 1473 K,[14,15] SiS_2 is at least tetramorphic. With higher pressure, the density (ρ) of SiS_2 increases. Upon the transformation of orthorhombic NP-SiS_2[9,10,12] (ρ_{calc} = 2.044(2) g cm^{-3} and 300(2) K; see Table S1 in the SI) to monoclinic SiS_2 at 2.8 GPa, the density increases by 8.8%, to ρ_{calc} = 2.241(2) g cm^{-3} (see Table S2 in the SI). Transformation of HP1-SiS_2 at 3.5 GPa to monoclinic HP2-SiS_2 increases ρ further by 4.4% to 2.344(2) g cm^{-3} (Table S3 in the SI). The same holds true for the transition of HP2-SiS_2 at 6 GPa[14,15] into tetragonal HP3-SiS_2 which increases ρ by 1.1%, to 2.37(5) g cm^{-3}. It is interesting to clarify the structural background for these transformations of the NP phase to the HP1 (2.8 GPa), HP2 (3.5 GPa), and HP3 phase (6 GPa).[14,15] HP1-SiS_2 is a layer structure, exhibiting a two-dimensional arrangement of distorted SiS_4 tetrahedra with sharing of one edge and two corners in the *b*–*c* plane. In comparison to orthorhombic NP-SiS_2, where one-dimensional interbonding of tetrahedra occurs only in the *c*-direction, in HP1-SiS_2, a second dimension (the *b*-direction) was "activated".

In Figure 2a, Guinier diffractograms (Mo Kα_1 radiation) of HP1-SiS_2 from 6° to 46° (2θ) (T = 293(2)–701(5) K) are given. Figure 2b shows the relative change (%) of lattice parameters *a*, *b*, and *c* and cell volume *V* at temperatures up to 701 K. Figures 2c and 2d show two Diamond2 views[27] of this phase at 293 K along the [010] and [100] axes, respectively. Distances and angles at 293(2) K are summarized in Figure 2e.

Layers of tetrahedra with strong chemical bonding are found in the *b*–*c* plane. In these directions, thermal expansion is the lowest. In the *a*-direction, the layers are stacked. Indeed, here, thermal expansion is about two times higher than for *b* and *c* (Figure 2b). The ADP follows this tendency. Strong bonding is also reflected in small displacement parameters. For the Si and the S(1) and S(2) atoms, displacement parameters U_{33} and U_{22} are ~75% of U_{11} (see Table S2 in the SI). Since thermal expansion for the *c*-direction is lower than for *b*, U_{33} is lower than U_{22} in two of three cases. This indicates that, here, bonding in the *b*–*c* plane is the strongest and distorted SiS_4 tetrahedra are connected in two-dimensional layers parallel to (011).

The structural motif of 12-membered rings with two pairs of edge-connected tetrahedra and two corner-shared tetrahedra is also found in $Nd_4N_2Se_3$, which is a neodymium(III) nitridoselenide with distorted $[NNd_4]^{9+}$ tetrahedra.[28] In addition, edge- and corner-sharing tetrahedra have also been observed nitridosilicates, e.g., $La_{16}[Si_8N_{22}][SiON_3]_2$[29] with isolated $[SiON_3]^{7-}$ tetrahedra and infinite chains of $[Si_8N_{22}]^{34-}$, consisting of both edge- and corner-sharing SiN_4 tetrahedra.

Nevertheless, the lattice parameters *a*, *b*, and *c* and the unit-cell volume *V* clearly show a positive thermal expansion (Figure 2b). The U_{ii} displacement values for NP-SiS_2 (i = 3, and T = 300(2) K; see Table S1 in the SI) and for HP1-SiS_2 (i = 2, 3, and T = 293(2) K) (see Table S2 in the SI) reveal that NP-SiS_2, in the *c*-direction, is stronger-bonded than HP1-SiS_2 in the *b*- and *c*-directions.

A further increase in density could be possible when the van der Waals gap between the two-dimensional layers in HP1-SiS_2 is replaced by strong chemical bonds. With this, a three-dimensional arrangement of SiS_4 tetrahedra would be created. Indeed, this is realized in HP2-SiS_2, again with edge- and corner-sharing distorted SiS_4 tetrahedra. In comparison to HP1-SiS_2, the unit-cell volume of HP2-SiS_2 is tripled (see Table S3 in the SI). As a result, this structure is built up by three crystallographic different Si and six crystallographic different S atoms which form puckered 12-membered Si_6S_6 rings with edge- and corner-sharing distorted SiS_4 tetrahedra.

Figure 3a shows Guinier diffractograms (Mo Kα_1 radiation) of HP2-SiS_2 from 6° to 46° (2θ) and T = 295(2)–716(5) K. Figure 3b depicts the relative change (%) of lattice parameters *a*, *b*, and *c* and of the cell volume *V* at various temperatures. Figure 3c displays two puckered Si_6S_6 rings, centered in the projection on the (101) plane at a = 0, c = 1/2, with seven approximately planar Si_2S_4 rings for edge-sharing and eight S atoms for corner-sharing of tetrahedra. In the unit cell of HP2-SiS_2 (Figure 3d), such 12-membered rings are centered in the projection on the (101) plane, here at a = 0, c = 0 and at a = 0, c = 1. Figure 3e shows distances (Å) (experimental error ±0.002) and angles (deg) (experimental error ±0.02) in a view on a 12-membered Si_6S_6 ring built up by six SiS_4 tetrahedra. A 12-membered ring consisting of six tetrahedra is also found in HP1-SiS_2 (recall Figures 2d and 2e).

Figure 3a shows the Guinier diffractograms of HP2-SiS_2 (Mo Kα_1 radiation) from 6° to 46° (2θ) and T = 295–716 K. Figure 3b shows that the lattice parameters *a*, *b*, and *c* and the cell volume *V* at various temperatures expand positively. However, thermal expansion is the lowest for parameter *c*, and that for parameters *b* and *a* is slightly higher. Inspection of the U_{ii} ADP (see Table S3 in the SI) reveals that the average U_{11} parameters for the Si and S atoms are the largest and the U_{33}

DOI: 10.1021/ic501825r
Inorg. Chem. 2015, 54, 1240–1253

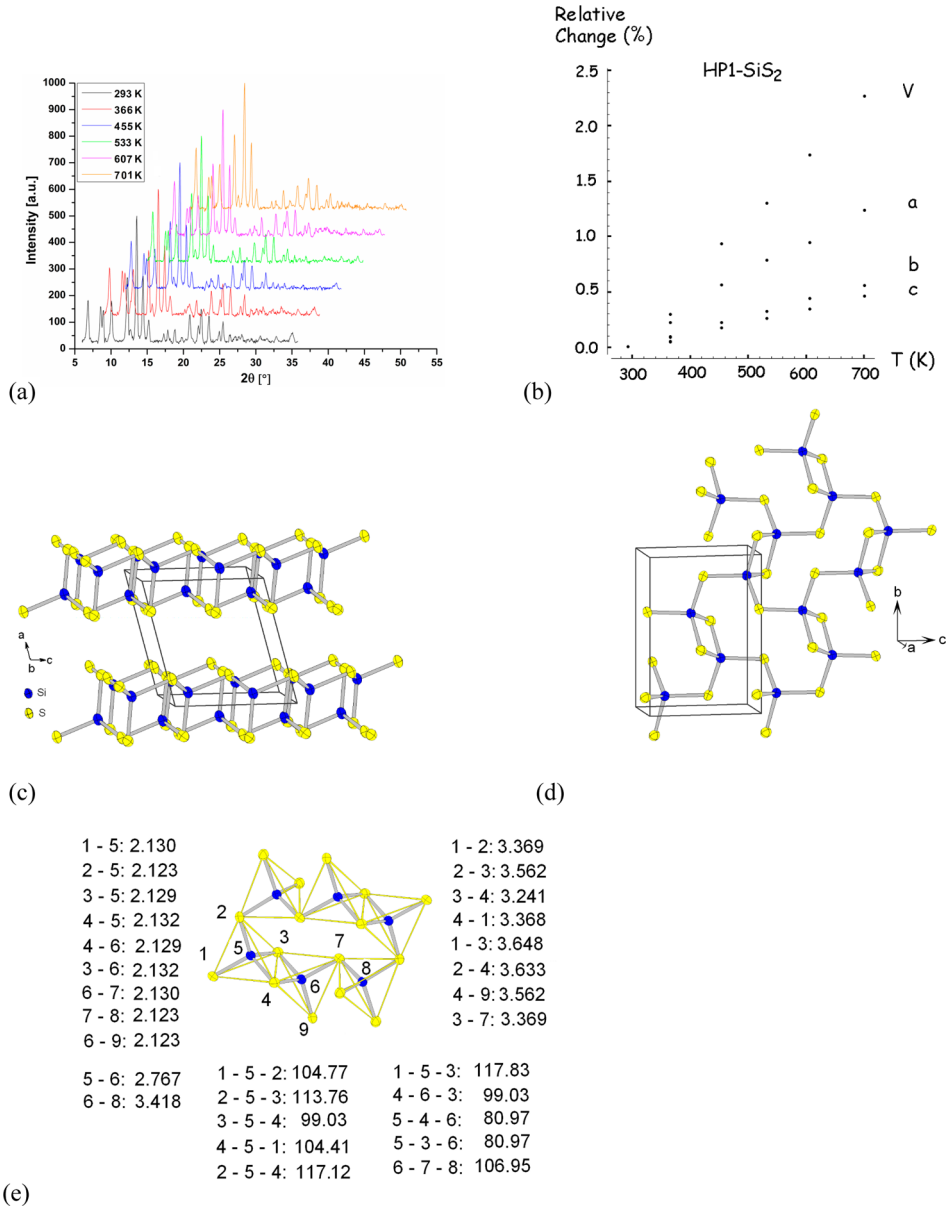

Figure 2. (a) Guinier diffractograms (Mo Kα_1 radiation) of HP1-SiS_2 from 6° to 46° (2θ), with an increment of 0.04° and a counting time of 10 s per increment from 293(2) K to 701(5) K. (b) Relative change (%) of the lattice parameters *a*, *b*, and *c* and of the cell volume (*V*) at various temperatures. (The data at 293(2) K were obtained by single-crystal X-ray analysis (see Table S2 in the SI), and those data up to 701(5) K were obtained by Guinier powder X-ray investigation. HP1-SiS_2 shows no negative NTE in the investigated temperature range; the thermal expansion of *c* and *b* is the lowest.) (c) Diamond2 view[27] of HP1-SiS_2 at 293(2) K along the [010] axis with anisotropic displacement ellipsoids of 50% probability, showing that the layer structure consisted of edge- and corner-shared distorted SiS_4 tetrahedra. (The highest displacements of the ellipsoids are parallel to [100], indicating only weak van der Waals forces between the layers. Perpendicular to (011) the layers of tetrahedra are stacked with an A, B, C, D··· sequence.) (d) View along the [100] axis on one layer of distorted SiS_4 tetrahedra with four 12-membered Si_6S_6 rings. (e) View on a 12-membered Si_6S_6 ring formed by six distorted SiS_4 tetrahedra. (Distances (Å) and angles (deg) (experimental errors of ±0.002 Å and ±0.02°, respectively) obtained via single-crystal X-ray determination (see Table S2 in the SI) at 293(2) K are summarized. The Si−Si distances between edge-sharing tetrahedra (Si5, Si6) are elongated from 2.767(2) Å to 3.418(2) Å for corner-sharing ones (Si6, Si8). The corner-sharing angle Si−S−Si (6−7−8) is 106.95(2)°.)

parameters are the smallest. These facts are reflected in the thermal expansion of the lattice parameters for *a*, *b*, and *c* (Figure 3b).

Contrary to the Si−S distances in HP1-SiS_2, which are found only in a small interval between 2.123(2) Å and 2.132(2) Å, they lie in HP2-SiS_2 in a larger interval between 2.124(2) Å and 2.143(2) Å (see Figure 3e). On the one hand, HP1-SiS_2 consists of only one crystallographic independent Si and two independent S positions (see Table S2 in the SI). On the other hand, in HP2-SiS_2, those atoms are tripled (see Table S3 in the SI).

Because the Si−S distances and the Si−S−Si angles in distorted SiS_4 tetrahedra and also the angles Si−S−Si at the interconnection by corner-sharing in HP1- and HP2-SiS_2 deviate only slightly from each other in HP1-SiS_2 and in HP2-SiS_2, the volumes of the distorted SiS_4 tetrahedra in both phases are very similar. Nevertheless, edge-sharing and corner-sharing of distorted tetrahedra in HP2-SiS_2 (ρ_{calc} = 2.344(2) g cm^{-3})

DOI: 10.1021/ic501825r
Inorg. Chem. 2015, 54, 1240−1253

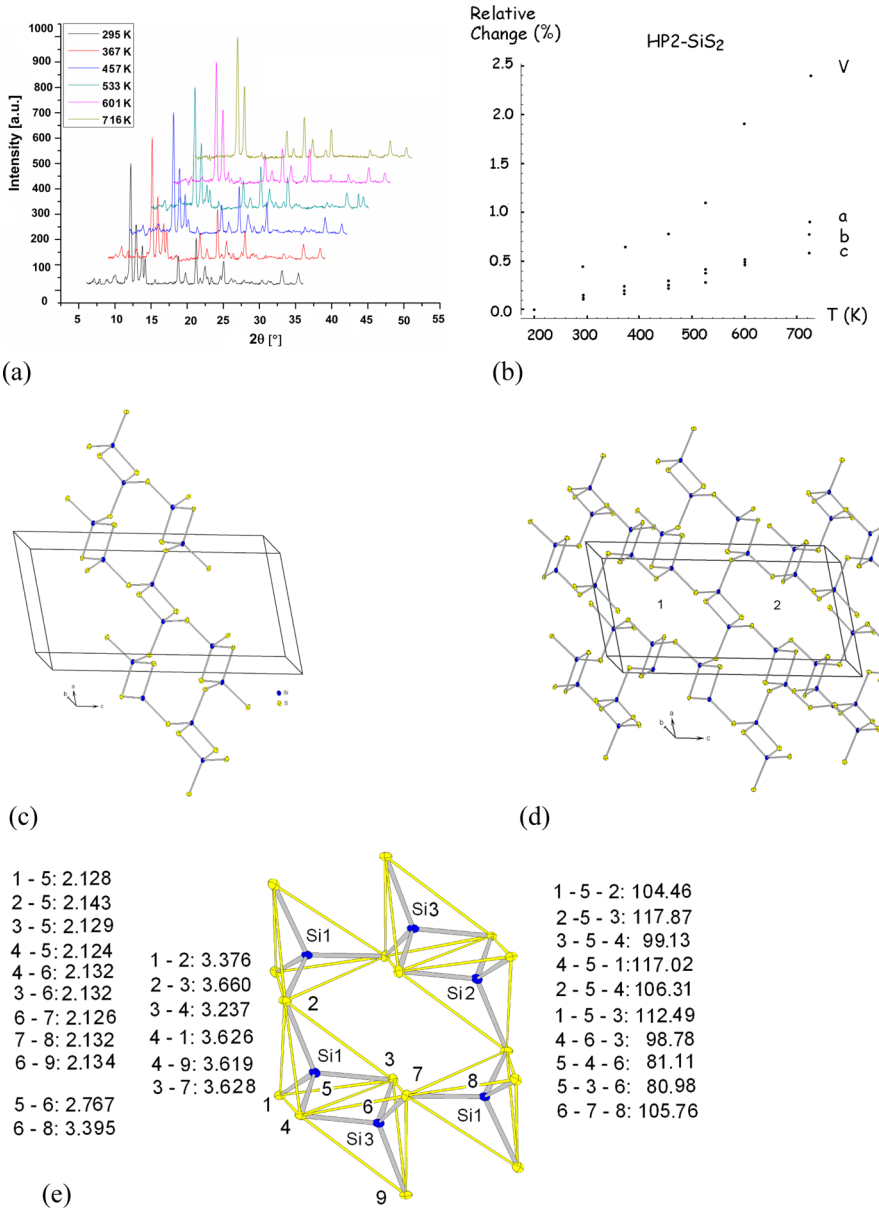

Figure 3. (a) Guinier diffractograms (Mo Kα_1 radiation) of HP2-SiS_2 from 6° to 46° (2θ) with an increment of 0.04° and a counting time of 10 s (T = 295(2)−716(5) K). (b) Relative change (%) of the lattice parameters a, b, and c and of the cell volume (V) at various temperatures. (The data at 200(2) K were obtained via single-crystal X-ray analysis (see Table S3 in the SI), those data up to 716(5) K were obtained via Guinier powder X-ray investigations. HP2-SiS_2 shows no negative thermal expansion (NTE) in the investigated temperature range; the thermal expansions in the a-, b-, and c-directions are approximately in the same range. (c) Diamond2 view[27] along the [010] axis (displacement ellipsoids with 50% probability) on edge- and corner-sharing distorted SiS_4 tetrahedra of HP2-SiS_2 centered at a = 0, c = 1/2. (Two puckered Si_6S_6 rings are obtained by connection of seven approximately planar Si_2S_2 rings.) (d) View along the [010] axis with the structural motif of puckered Si_6S_6 rings of Figure 2b, but centered here at c = 0 and c = 1. (e) View on a 12-membered ring Si_6S_6 of six SiS_4 tetrahedra. Distances (Å) (experimental error ±0.002) and angles (deg) (experimental error ±0.02) as determined by single-crystal determination at 200(2) K (see Table S3 in the SI) are summarized for six SiS_4 tetrahedra of HP2-SiS_2. (The Si−Si distances between edge-sharing tetrahedra (Si5, Si6) are elongated from 2.767(2) to 3.395(2) Å for corner-sharing ones (Si6, Si8). The corner-sharing angle Si−S−Si (6−7−8) is 105.76(2)°.)

leads due the three-dimensional arrangement of SiS_4 tetrahedra to a more-efficient packing than in HP1-SiS_2 (ρ_{calc} = 2.241(2) g cm^{-3}).

In Figure 4, the packing in the a−c plane of distorted SiS_4 tetrahedra for HP1-SiS_2 and HP2-SiS_2 is compared. The gap between the layers of HP1-SiS_2 of 3.18 Å (Figure 4a) results from only weak van der Waals bonding and is 11% larger than the thickness of the layer (2.84 Å). In HP2-SiS_2 (Figure 4b), the S atoms of the SiS_4 tetrahedra lie approximately parallel to the (101) plane. In such an arrangement, chemical bonds in three dimensions reduce the distance to 2.84 Å (Figure 4b). This smaller distance seems to allow a more-efficient packing in HP2-SiS_2 than in HP1-SiS_2. Nevertheless, two large cavities remain. They are numbered as "1" and "2" in Figure 3d.

Tetragonal HP3-SiS_2. According to the Pauling rules,[30,31] the sharing of polyhedra edges reduces the stability of an ionic structure. DFT calculations of Bader partial charges[32,33] with WIEN2k[34] show a large valence electron transfer from the electropositive Si atoms to the electronegative S atoms. For the NP phase and the three HP-SiS_2 phases, the calculated partial

DOI: 10.1021/ic501825r
Inorg. Chem. 2015, 54, 1240−1253

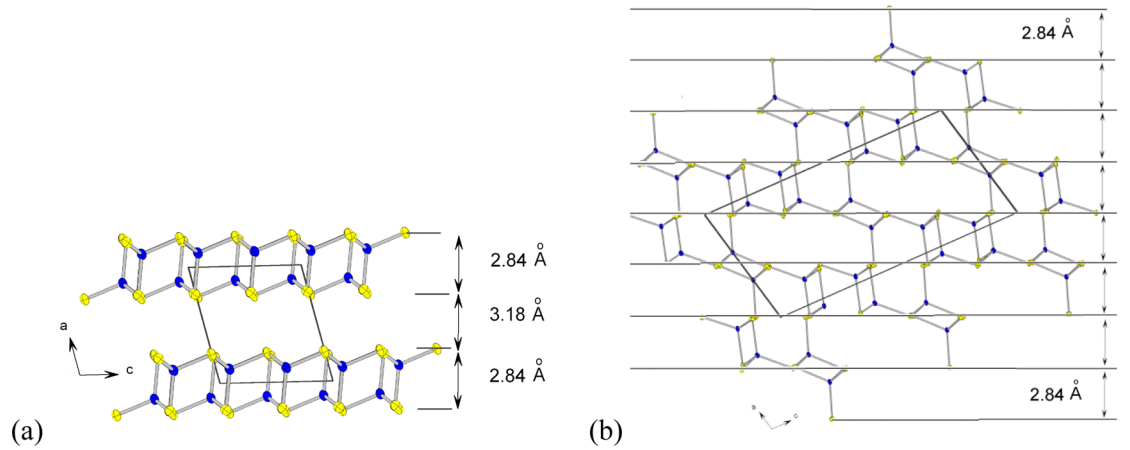

Figure 4. Diamond2 views[27] along the [010] axis on HP1-SiS_2 and HP2-SiS_2. In both structures, the Si−S, Si−Si, and S−S distances in the distorted tetrahedra are approximately equal (see Figures 2e and 3e): (a) in the layers, the gap between distorted tetrahedra in HP1-SiS_2 is 3.18 Å, their height is 2.84 Å; (b) in HP2-SiS_2, the layer gaps are filled by forming chemical bonds in a three-dimensional net (the tetrahedra are arranged in planes with smaller distances of only 2.84 Å, allowing a denser packing than in HP1-SiS_2; nevertheless, cavities remain, which are numbered as "1" and "2" in Figure 3d).

charge of the Si atoms lies between +3.1 and +3.2 and indicates strong ionic bonding. If the cell volume is compressed by 5%, comparable to a compression by ∼5 GPa, the Bader partial charges of the Si atoms increase by 2%, indicating a slightly stronger electron transfer from Si to S.

Therefore, a further increase in density, compared to NP-SiS_2 and to HP1-SiS_2 and HP2-SiS_2, is expected if sharing is applied to all four corners of a tetrahedron. This is realized in the tetragonal HP3-SiS_2. We obtained it at a pressure lower than that previously reported.[15] In this investigation, we present as well a refinement of the structural data of tetragonal HP3-SiS_2 with modern single-crystal X-ray techniques at 100(2), 200(2), 300(2), and 400(2) K, in order to determine the thermal expansion and the displacement parameters.

The crystallographic data are summarized in Table S4 in the SI. In Figure 5a, Guinier diffractograms (Mo Kα_1 radiation) of HP3-SiS_2 from 6° to 46° (2θ), at T = 300(2)−707(5) K, are shown. Figure 5b presents the relative change (%) of lattice parameters a and c and the cell volume V at various temperatures. The data at 100(2), 200(2), 300(2), and 400(2) K were obtained via single-crystal X-ray analysis (see Table S4 in the SI), and data up to 707(5) K were determined via Guinier powder X-ray investigations. In Figure 5c, Diamond2 views[27] of HP3-SiS_2 along the [100] axis with anisotropic displacement ellipsoids of 50% probability are summarized, showing that the corner sharing of distorted tetrahedra builds a network. In Figure 5d, a view is shown on 16 distorted tetrahedra of HP3-SiS_2 along the [010] axis at T = 300(2) K with S−S distances in corner-sharing distorted SiS_4 tetrahedra (with large voids between them). In Figure 5e, a view on five distorted SiS_4 tetrahedra of HP3-SiS_2 along the [010] axis with the distances (Å) and angles (deg) noted, is shown (experimental errors of ±0.002 Å and ± 0.02°, respectively).

In 1965, Prewitt and Young had performed their investigation at room temperature.[15] Their lattice parameters a and c (5.420(4) Å, 8.718(4) Å), their positional parameter x_S (0.2272(4)), and their isothermal displacement parameters $U_{eq,Si}$ and $U_{eq,S}$ (0.0091(20) Å^2, 0.0166(20) Å^2) deviate slightly from our data at 300(2) K (see Table S4 in the SI). Figure 5b shows that thermal expansion of the lattice parameters a and c and the unit-cell volume change is negative in the interval between 100(2) K and 200(2) K. Up to 707(5) K, the increase in V is ∼2% and that of a is 0.8%. This small expansion of a is in the range also observed for parameters a, b, and c in HP2-SiS_2. The lattice parameter c observed in the range of 200(2)−707(5) K shows no clear thermal expansion, but it is almost zero above 300 K (Figure 5b). The variation of V, a, and c for HP3-SiS_2 is the smallest in the investigated temperature range for tetramorphic SiS_2, e.g., $\Delta V_{NP\text{-}SiS_2}$ = +7.0% (Figure 1b), $\Delta V_{HP1\text{-}SiS_2}$ = +2.3% (Figure 2b), $\Delta V_{HP2\text{-}SiS_2}$ = +2.4% (Figure 3b), $\Delta V_{HP3\text{-}SiS_2}$ = +2.0% (Figure 5b). These results suggest that HP3-SiS_2 is the most rigid, in comparison to NP-, HP1-, and HP2-SiS_2, because of its complex three-dimensional net. In addition, the ADP U_{ii} values for HP3-SiS_2 at 100(2) K are very low (e.g., $U_{Si,11}$ = 0.0060(6), $U_{Si,33}$ = 0.0042(6) Å^2; see Table S4 in the SI). Compared to those in NP-SiS_2, they are nearly halved (e.g., $U_{Si,11}$ = 0.0139(4), $U_{Si,33}$ = 0.0100(3) Å^2; recall Table S1 in the SI). However, between 100(2) and 400(2) K, there is no clear tendency in HP3-SiS_2, regardless of whether the ADP U_{11} or U_{33} (Table S4 in the SI) is smaller.

The Si−S distances in HP3-SiS_2 within the tetrahedra are 2.135(2) Å (Figure 5e), as they have been approximately also observed in NP-SiS_2 (2.130(2) Å (Figure 1e), in HP1-SiS_2 (2.123(2)−2.132(2) Å (Figure 2e)) and in HP2-SiS_2 ((2.128(2)−2.134(2) Å) (Figure 3e)). The sum of ionic radius of Si and S (0.26 Å for Si^{4+} in tetrahedral coordination and 1.84 Å for S^{2-})[35] is consistent with the present experimental distances Si−S. The tetrahedra angles lie between 105.08(2)° and 118.65(2)°. The corner-sharing Si−S−Si angle is 109.63(2)°, which is ∼3° larger than that for HP1- and HP2-SiS_2. The S−S edges of the tetrahedra are 3.389(2) and 3.673(2) Å (Figure 5e).

Group−Subgroup Relationships between SiS_2 Phases. It is well-known that the group−subgroup relationships, as represented in Bärnighausen trees,[36−44] indicate common features between crystal structures. Such a Bärnighausen tree is shown in Figure 6 for NP-, HP1-, HP2-, and HP3-SiS_2. The top of the tree is formed by the fluorite (CaF_2) structure (space group $F4/m\bar{3}2/m$, with a lattice parameter of a = 5.462 Å)[45] as aristotype. In CaF_2, the Ca atoms occupy the positions of cubic close-packed atoms in (0,0,0) and the F atoms those of

DOI: 10.1021/ic501825r
Inorg. Chem. 2015, 54, 1240−1253

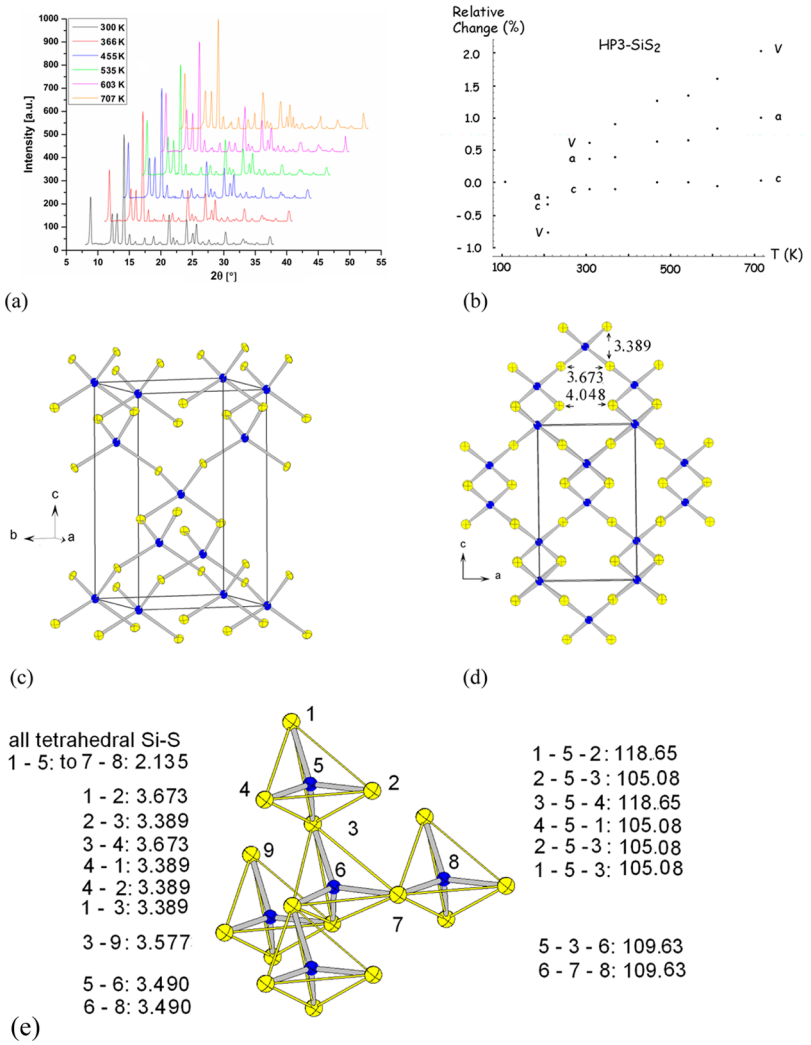

Figure 5. (a) Guinier diffractograms (Mo Kα_1 radiation) of HP3-SiS_2 from 6° to 46° (2θ) with an increment of 0.04° and a counting time of 10 s per increment (T = 300(2)−707(5) K). (b) Relative change (%) of lattice parameters a, c, and cell volume V at various temperatures. (The data at 100(2), 200(2), 300(2), and 400(2) K were obtained via single-crystal analysis (see Table S4 in the SI), whereas data up to 707(5) K were obtained via Guinier diffractograms. HP3-SiS_2 shows that a negative NTE is observed only in the temperature range of 100(2)−200(2) K (see Table S4 in the SI). Up to 707(5) K, parameter c shows lower, but slightly positive, thermal expansion. For parameter a, the thermal expansion is in the same range as parameters a, b, and c in the three-dimensional net of HP2-SiS_2.) (c) Diamond2 view[27] of HP3-SiS_2 along the [100] axis with anisotropic displacement ellipsoids of 50% probability at 300(2) K (Table S4 in the SI), showing that the corner sharing of distorted tetrahedra builds a network. (d) View on 16 distorted tetrahedra of HP3-SiS_2 along the [010] axis at 300(2) K with S−S distances in corner-sharing distorted SiS_4 tetrahedra with large voids between them. (e) Distances (Å) and angles (deg) (experimental errors of ±0.002 Å and ±0.02°, respectively) for tetragonal HP3-SiS_2 are summarized (data taken from Table S3 in the SI).

tetrahedral holes in ($^1/_4$,$^1/_4$,$^1/_4$). In the left branch of the tree, the relationship to NP-SiS_2 is derived, followed by the relationship to HP1-SiS_2 and HP2-SiS_2 and to HP3-SiS_2 on the right branch.

Coming from CaF_2, the larger S atoms of SiS_2 adopt the part of the Ca atoms for close-packed positions and the Si atoms adopt those of the F atoms. To obtain NP-SiS_2, the first step[38,44] leads to a *translationsgleich* subgroup $F4/m\,2/m\,2/m$ of index 3, which is a nonstandard setting of $I4/mmm$. By this F-setting the larger lattice parameter a of NP-SiS_2 (a = 5.5528 Å) is retained. By two *klassengleich* symmetry reduction steps of index 2 (Figure 6), two origin changes with ($^1/_4$,$^1/_4$,$^1/_4$) and ($-^1/_4$,0,0), and doubling the lattice parameter b, the space group $I2/m2/c2/b$ of NP-SiS_2 is obtained. The positions of the tetrahedral holes of the aristotype CaF_2 are not changed in NP-SiS_2, bearing in mind the two origin changes. The positions of the S atoms are slightly shifted (for y= −0.250 to y= −0.206, and for z = −0.125 to z = −0.117 (Figure 6)).

The symmetry reduction[39] to obtain HP1-SiS_2 and HP2-SiS_2 from the aristotype CaF_2 includes five common steps via $I4/mmm$ (t3), $P4_2/nnm$ (k_2), $P2/n\,2/n\,2/n$ (t2), $P12/n1$ (t2) to $P12_1/n1$ (k2). Then, after changing the cell parameters, the middle branch of the tree is divided into two parts, both in space group $P12_1/c1$. For HP1-SiS_2, the new cell vectors $\boldsymbol{a} - \boldsymbol{c}$, $\boldsymbol{b}$, $\boldsymbol{a} + \boldsymbol{c}$ are chosen with an i2 reduction step. The positional parameters for HP1-SiS_2 deviate only slightly from the ideal ones, based on multiples of 1/8 (Figure 6). The deviation of the positional parameters for HP2-SiS_2, on the right side of the middle branch, is also very small. Here, the x positional parameters are based on 1/(8 × 3) = 1/24, because of the tripling of lattice vectors in the steps $\boldsymbol{a}$, $\boldsymbol{b}$, $-\boldsymbol{a}+3\boldsymbol{c}$, and $2\boldsymbol{a},\boldsymbol{b},\boldsymbol{c}$

DOI: 10.1021/ic501825r
Inorg. Chem. 2015, 54, 1240−1253

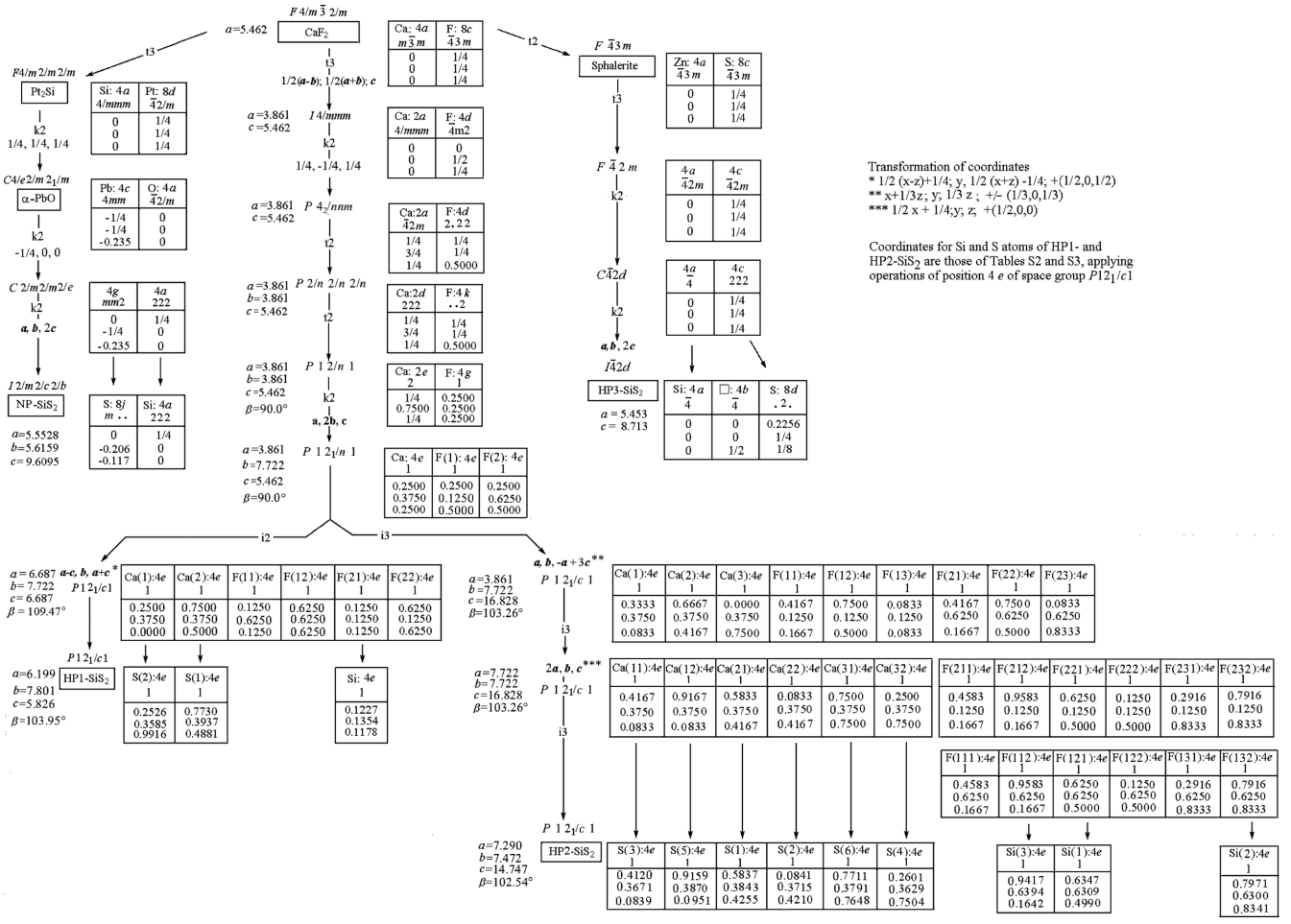

Figure 6. Bärnighausen tree for group−subgroup relationships between the fluorite (CaF_2) structure as aristotype and the crystal structures of NP-SiS_2, HP1-SiS_2, HP2-SiS_2, and HP3-SiS_2.[36−44]

(Figure 6). In HP1-SiS_2 and in HP2-SiS_2, all positions of the original close-packed Ca atoms in CaF_2 are occupied by S atoms in SiS_2 (HP1:2, HP2:6, respectively). Because of the 1:2 stoichiometry, the Si atoms in HP1-SiS_2 occupy only 1 of 4 tetrahedral positions and, in HP2-SiS_2, only 3 of 12 tetrahedral positions. The unoccupied tetrahedral positions are equivalent and do not open new structural arrangements.

HP3-SiS_2 is derived from the aristotype CaF_2 via the non-centrosymmetric sphalerite (ZnS) structure,[38,44] three additional steps (*t*3, *k*2 (2*x*)), and doubling the lattice parameter *c*. Hereby, the positional parameter *x* of the S atoms is only slightly shifted from the ideal value of $x = 0.250$ to $x = 0.226$. The Si position remains unchanged at (0,0,0).

It has been already shown that the four SiS_2 phases contain Si atoms in tetrahedral holes with a coordination number of 4. However, with increasing pressure—probably in the range of 10−20 GPa—a SiS_2 phase with a silicon coordination number of 6 (i.e., in SiS_6 octahedra) could be stabilized. High-pressure experiments with SiS_2, applying multianvil and also diamond anvil cell techniques, are currenty underway.

Vibrational Spectroscopy of the SiS_2 Phases. The Raman spectroscopic results of the four SiS_2 phases are collected in Table 1 (excitation wavelength = 514.5 nm). In order to illustrate the high quality of our samples, the Raman spectra of the four phases and visualization of the motions of the most intense bands are presented in Figure 7. After a first qualitative inspection, a red shift of the most intense bands at 434 (NP), 408 (HP1), 404 (HP2), and 324 cm^{-1} (HP3) is observed. Because of the fact that the compression of a material leads to an increase of the vibrational frequencies, we expected a blue shift among the different phases with increasing density ρ. Since this behavior was not observed in this case, we assume that the structural changes upon phase transitions might explain this apparent trend. Therefore, we performed solid-state DFT calculations for all four phases using the program system CRYSTAL06 (functional BP86, basis sets of 3-11G* quality for all atoms)[46] to investigate the change of the vibrational feature by a simple vibrational analysis.

The frequency calculations are based on the experimental geometries. The theoretical Raman active bands are listed in Table 1, together with the experimental data. All calculated vibrations fit very well with the experimental ones, especially with the most intense Raman bands discussed above. As expected, they belong to totally symmetric motions which are visualized in Figure 7.

Since the unexpected red shift of these bands with increasing density of the material is confirmed by the calculations, one must analyze the underlying vibrational equations. For these frequencies of the four phases, we have extracted model moieties, in which, in principle, the Si atoms are hardly involved, although both the Si and S atoms contribute equally to the G-matrix (representing the kinetic energy of the vibrational equations);[47] i.e., the observed and calculated drastic shifts of these frequencies are caused by different F-matrices (representing the

DOI: 10.1021/ic501825r
Inorg. Chem. 2015, 54, 1240−1253

Table 1. Theoretical and Experimental Raman Frequencies of Tetramorphic Solid SiS_2

ν(exp.) [cm^{-1}]	ν(theor.) [cm^{-1}]	representation	ν(exp.) [cm^{-1}]	ν(theor.) [cm^{-1}]	representation
	NP-SiS_2			**HP2-SiS_2**	
	26.6	B_{1g}		57.2	B_g
141.6	138.9	A_g	67.5	66.1	A_g
177.2	166.7	B_{3g}	73.6	75.9	B_g
185.0	180.3	B_{2g}		81.3	A_g
219.2	comb.		92.4	91.9	B_g
353.5	347.0	B_{1g}		93.1	A_g
433.9	444.8	A_g	100.9	102.3	A_g
449.1	453.8	B_{2g}	105.2	108.3	B_g
	454.5	B_{3g}	111.3	112.4	A_g
629.1	646.0	B_{1g}		113.4	B_g
			118.5	116.1	A_g
			122.8	120.1	B_g
			134.3	126.5	B_g
			137.9	131.2	A_g
			152.4	146.1	A_g
				147.2	B_g
				162.9	A_g
	HP3-SiS_2			165.1	B_g
			175.3	170.1	A_g
128.8	113.6	E	194.0	189.8	A_g
213.2	201.1	B_2		190.3	B_g
246.1	240.3	E		199.8	B_g
287.2	290.4	B_1	231.7	226.7	B_g
324.0	329.7	A_1	239.5	233.9	A_g
472.4	494.0	B_2	246.1	240.4	A_g
505.5	511.5	B_1	251.5	247.5	B_g
538.4	530.7	E	272.3	270.1	A_g
552.3	566.7	E	277.1	271.4	B_g
590.2	comb.		297.9	295.7	A_g
			305.0	303.5	B_g
			364.7	373.7	B_g
			383.5	390.6	A_g
			404.1	411.4	A_g
				415.5	B_g
	HP1-SiS_2		418.7	428.1	A_g
			440.9	433.0	B_g
80.9	66.7	A_g	450.3	465.4	A_g
96.7	76.6	B_g		467.1	B_g
120.3	107.7	A_g	477.6	475.1	A_g
148.2	138.7	A_g		475.3	B_g
	139.1	B_g		505.8	A_g
182.0	177.1	B_g		506.5	B_g
204.8	196.1	A_g	529	508.6	A_g
234.1	231.4	B_g	551	549.3	A_g
261.0	254.3	A_g		554.0	B_g
306.8	303.7	B_g		566.2	B_g
408.1	415.6	A_g		573.4	B_g
	436.1	B_g	574.1	574.5	A_g
438.5	464.1	A_g		596.4	A_g
	466.6	B_g		598.3	B_g
486.9	511.2	A_g	586.2	607.8	A_g
537.2	557.6	B_g		609.6	B_g
592.4	613.9	A_g	600.5	621.4	A_g
	617.2	B_g		626.3	B_g

potential energy of the vibrational equations)[47] (i.e., different restoring forces). If one concentrates on the NP and HP3 phases, their symmetric vibrations can be assigned to (a) those in a Si−S_2−Si four-membered ring (NP) and (b) those in a Si-centered SiS_4 tetrahedron (such as $SiCl_4$ molecules) (HP3). In both moieties, only the S atoms move.

DOI: 10.1021/ic501825r
Inorg. Chem. 2015, 54, 1240−1253

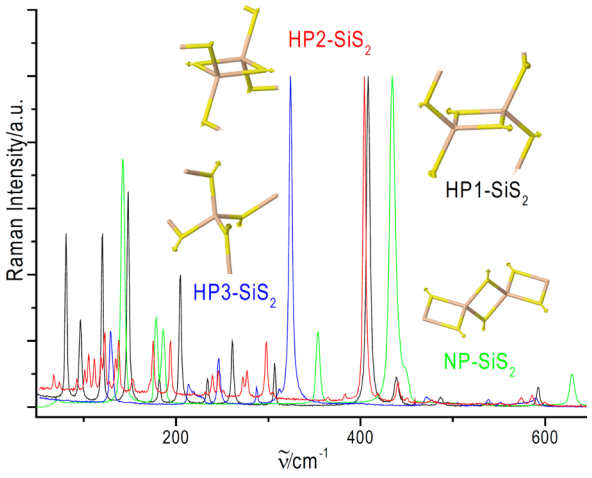

Figure 7. Raman spectra of tetramorphic SiS_2 (excitation wavelength = 514.5 nm). The visualization of the motions of the most intense Raman bands are also shown: NP, 434 cm^{-1}; HP1, 408 cm^{-1}; HP2, 404 cm^{-1}; and HP3, 324 cm^{-1}.

Symmetric Vibrations Assigned to Those in a Si−S_2−Si Four-Membered Ring (NP). In an earlier work on D_{2h} symmetric $(GeO)_2$ and $(NS)_2$ species,[47] we have extensively discussed the motions of these molecules, with respect to the G- and F-matrix. To summarize these discussions for the following argumentation, an extremely large F-matrix element results[48] (i.e., there are strong restoring forces for the motion of the S atoms). For the NP phase, this motion can be described as a chain of silent Si atoms in which the vibrating S atoms (perpendicular to the chain atoms) cause an increasing and decreasing diameter of a "SiS_2 wire". In a simple vision, the restoring force, i.e., the bond strength of each SiS bond, is increased via interaction by the other SiS bonds in the Si_2S_2 ring. Therefore, this force constant F of the NP phase reflects a delocalized bonding for all four SiS bonds. In order to quantify this increase of the force constant F, one must conclude from the discussion of typical molecular A_2B_2 ring systems (Al_2Cl_2, Si_2O_2, Ge_2O_2)[47] that the interaction part (f_{rr}, f'_{rr}, f''_{rr}) of this symmetric vibration of the Si_2S_2 moiety increases the stretching force constant F_{SiS} by ∼40%, resulting in the high A_g mode at 434 cm^{-1}.

Symmetric Vibrations Assigned to Those in a Si-Centered SiS_4 Tetrahedron (Such as $SiCl_4$ Molecules) (HP3). On the other hand, the $SiCl_4$-like motion in the HP3 phase at 324 cm^{-1} is only influenced by the force constant $F = f_{SiS} + 3f_{(SiS/SiS)}$. Similar to that observed in every tetrahedral XY_4 molecule, the bond−bond interaction force constants are small (i.e., the value of f_{SiS} is increased by three small identical $f_{(SiS/SiS)}$ interaction constants, which results in an increase of ∼12%).[49] Therefore, the different values of the force constant of the NP and the HP3 phase should be the main reason for the unexpected frequency shift within the totally symmetric motion.

The values of the most intense Raman frequencies of the HP1 and HP2 phases containing corner-sharing, as well as edge-sharing moieties—408 and 404 cm^{-1}—are expected to be between those of the NP and HP3 phases.

3. CONCLUSION AND OUTLOOK

The following conclusions are made from these studies:

- Via single-crystal X-ray investigations, since 1991, two unknown structures of SiS_2 have been solved.[17] HP1-SiS_2 and HP2-SiS_2 are monoclinic and consist of distorted SiS_4 tetrahedra, which are edge-sharing and also corner-sharing. Both phases represent the missing links between NP-SiS_2, with only edge-sharing tetrahedra, and HP3-SiS_2, with only corner-sharing tetrahedra.
- The structures in tetramorphic SiS_2 have been investigated by single-crystal X-ray investigations. Together with Guinier powder X-ray investigations, it was revealed that, in tetramorphic SiS_2, up to 700 K, no negative thermal expansion (NTE) is observed. The determination of ADP obtained by single-crystal investigations allow a better understanding of the thermal expansion of the lattice parameters a, b, and c, up to 700 K.
- In tetramorphic SiS_2, the density increases if the applied pressure rises, considering NP-SiS_2 (0.0001 GPa), HP1-SiS_2 (2.8 GPa), HP2-SiS_2 (3.5 GPa), and HP3-SiS_2 (4.0 GPa). Although a three-dimensional arrangement of corner-sharing SiS_4 tetrahedra is present in HP3-SiS_2, large cavities are found.
- A large increase of the density may be possible if the applied pressure is increased up to 10−20 GPa. At such pressures, the tetrahedral SiS_4 coordination could be increased to an octahedral SiS_6.
- The Raman spectroscopic data of tetramorphic SiS_2 show a surprising effect. With increasing pressure, a blue shift is expected for the most intense bands. However, the observed unexpected red shift with increasing pressure is confirmed by DFT calculations. The values of the force constants, which are strongly influenced by different bond−bond interaction, for NP-SiS_2 (with only edge-sharing SiS_4 tetrahedra) and HP3-SiS_2 (with only corner-sharing tetrahedra) are the main reason for the band shift of the totally symmetric vibration. Since the HP1 and HP2 phases are the missing links between the NP and HP3 phases, the most intense Raman bands of the first lie between those of the second.

4. EXPERIMENTAL DETAILS

Synthesis of the Ambient Pressure Phase (NP). The NP phase of SiS_2 was obtained by reaction of high-purity silicon and sulfur in a ratio of 1:2.2 in a closed silica tube at temperatures of 773−1073 K. Before reacting these elements, the empty silica tube was thoroughly dried by heating it to 1273 K under high-vacuum (HV) conditions. In a glovebox with purified argon, the reactands were filled into the tube and then sealed off under HV. Direct contact of silicon and sulfur was avoided. Initially, a prereaction was performed by slowly heating the reactands to 773 K for 3 days. Using this procedure, sulfur from the vapor phase reacted with silicon and an explosion was avoided. Then, the reaction temperature was increased within 3 days to 1073 K, using a temperature gradient of 50 K between the cold end and the hot end of the reaction tube. This maximum temperature was maintained for an additional 3 days. Then, the temperature of the empty side of the ampule was reduced to 973 K, so that SiS_2 was sublimed within 3 days. Finally, the tube was slowly cooled to room temperature and opened in the glovebox, because SiS_2 is moisture-sensitive. Pure fibrous colorless crystals of NP-SiS_2 (∼4 mm in length) were found in the low-temperature (LT) part of the silica tube.

Transformation at High Pressure and High Temperature. In a belt apparatus, the HP phases of SiS_2 were prepared in boron nitride (BN) crucibles within cylindrical graphite

DOI: 10.1021/ic501825r
Inorg. Chem. 2015, 54, 1240−1253

heaters. For the starting experiments, typical conditions were 2−4 GPa and 1073−1473 K for 15 min and subsequent decompression after quenching to room temperature. Technical details of the experimental equipment and the pressure temperature calibration have been given elsewhere.[50,51] Special care was applied to maintain constant high-pressure conditions, since two different HP phases were obtained in small range of existence. Automatic indexing of 20 reflections of the two different HP phases with the program DICVOL[52] showed that, at 2.8 GPa and 1473 K, a first monoclinic phase (HP1-SiS_2), with lattice parameters a = 6.202(5) Å, b = 7.802(5) Å, c = 5.825(5) Å, and β = 104.0(5)° and at 3.5 GPa and 1473 K, a second monoclinic phase (HP2-SiS_2), with lattice parameters a = 7.290(5) Å, b = 7.475(5) Å, c = 14.750(10) Å, and β = 102.6(5)° was obtained. The reliability indices FN_{20}[53] are 15 and 11, respectively. Because of numerous overlapping reflections, the values of these monoclinic phases are lower than those for the orthorhombic NP-SiS_2 phase (FN_{20} = 25) and the tetragonal HP3-SiS_2 phase (FN_{20} = 25). The lattice parameters and the intensities of the Guinier diffractograms of HP1-SiS_2 and HP2-SiS_2 reproduce the data that Silverman and Soulen published in 1965 without indexing. The monoclinic HP1 phase was obtained at 2.8 GPa and 1473 K, whereas to the monoclinic HP2 phase was obtained at 3.5 GPa and 1473 K. At 4.0 GPa and 1473 K, single crystals of the tetragonal HP3-SiS_2[14,15] were also successfully prepared.

Powder Preparation. X-ray capillaries (0.5 mm diameter) of the four different SiS_2 phases (orthorhombic NP[9,10,12] new HP1-SiS_2, new HP2-SiS_2, and tetragonal HP3-SiS_2[14,15]) were filled in the glovebox and sealed. Special care had to be applied for the HP phases in order to scrape off the BN (residue from the walls of the crucibles used for the belt experiments). The white color of BN is not very different from that of the slightly yellow-brown HP phases.

Single-Crystal Preparation. From the NP-SiS_2 and HP-SiS_2 phases, ∼10−20 mg were covered on a watch glass with dried paraffin oil in the glovebox. Outside of the glovebox, several crystals were selected for examination under a microscope. Great care was taken to avoid contact with air and moisture. Considerable effort was exerted to isolate single crystals from the two new HP phases. They did not show well-developed faces. With rotation and Weißenberg X-ray photographs, two suitable single crystals could be separated from the microcrystalline material. In these cases, a crystallization time of several hours at high pressure was applied for the belt experiments.

Powder X-ray Experiments. Investigations were performed on a Huber Model G644 Guinier diffractometer with Mo Kα_1 radiation (λ = 0.7093 Å, quartz monochromator) in Lindemann capillaries (0.5 mm diameter). The angle calibration of the diffractometer was performed with electronic-grade germanium (a = 5.6575 Å). In the 2θ range between 4° and 34° with an increment of 0.04°, 750 data points were collected with a typical counting time of 10 s per increment. With a Huber heating attachment, heating and cooling cycles between 298 K and 773 K were performed. The temperature was calibrated by measuring Guinier diffractograms with NaCl between room temperature and 773 K under the same conditions as for SiS_2 samples. The variation of the lattice parameter of NaCl with temperature is tabulated.[54] The Guinier diffractograms obtained of the SiS_2 samples were investigated in the Rietveld technique with the program FULLPROF.[55]

Single-Crystal X-ray Diffraction Experiments. *NP-SiS_2.* A single crystal with dimensions of 0.50 mm × 0.05 mm × 0.04 mm was investigated with Mo Kα (λ = 0.71073 Å) in the temperature range between 100 K and 400 K using an Oxford Diffraction LTD Xcalibur3 diffractometer with a Cryojet Controller. A total of 1155 reflections with various hkl values were measured: h values between +13 and −13, k values between +8 and −6, and l values between +6 and −7.

HP1-SiS_2. A single crystal with dimensions 0.19 mm × 0.13 mm × 0.04 mm was investigated at 293(2) K with Mo Kα (λ = 0.71073 Å) using a STOE-IPDS single-crystal diffractometer. In these experiments, 1167 reflections with various hkl values were measured: h values between +8 and −8, k values between +10 and −10, and l values between +7 and −7.

HP2-SiS_2. A single crystal with dimensions 0.18 mm × 0.12 mm × 0.06 mm was investigated with Mo Kα (λ = 0.71073 Å) at 200(2) K, using a STOE IPDS single-crystal diffractometer. In these experiments, 2447 reflections with various hkl values were measured: h values between +7 and −7, k values between +7 and −7, and l values between +15 and −15.

HP3-SiS_2. A single crystal with dimensions 0.042 mm × 0.037 mm × 0.031 mm was measured in the temperature range from 100(2) K to 400(2) K, using an Oxford Diffraction LTD Xcalibur3 diffractometer with an Cryojet Controller. A total of 448 reflections with various hkl values were examined: h values between +5 and −6, k values between +6 and −4, and l values between +9 and −10. The structures of NP-SiS_2, HP1-SiS_2, HP2-SiS_2, and HP3-SiS_2 were solved using SHELXS-97 and refined using SHELXL-97.[56]

The angle calibration of the single-crystal diffractometers were performed with a BRUKER calibration "Ylid" crystal (dimethylsulfuranyliddiene-1.3-indandione) with lattice parameters of a = 5.9501(6) Å, b = 9.0360(8) Å, and c = 18.3522(18) Å at 300 K, with XYZ-centroids of 3671 reflections observed in the region of 2.51° < θ < 25.08° with Mo Kα radiation (0.71073 Å).[57]

DFT Calculations. Such calculations (total energy, as a function of unit-cell volume, Bader partial charges) were performed with the WIEN2k program[34] with the Generalized Gradient Approximation (GGA), potential 11, GMAX = 8, constant radii r_{MT} = 1.50 a.u., and a sufficient number of k-points (750 points for NP-SiS_2, 1000 points for HP1-SiS_2, 500 points for HP2-SiS_2, and 2000 points for HP3-SiS_2). Vibrational frequencies of all solid-state phases were calculated, based on the experimental geometries, using the program system CRYSTAL06 (DFT, functional BP86, basis sets of 3-11 G* quality for all atoms).[46]

The Raman intensities were not calculated by the CRYSTAL06 program. Therefore, the attribution of experimental Raman signals to the calculated ones was achieved by consideration of the irreducible representation to which they belong: (a) except for HP3-SiS_2, calculated vibrational signals of "u"-character are Raman inactive, because of the rule of mutual exclusion, and (b) we assume that the totally symmetric vibrations are presumably those of the highest Raman intensity. Because of the high quality of both the experimental and calculated spectra, this attribution appears highly reliable.

Raman Spectroscopy. The Raman spectra were recorded with the aid of a Dilor Model XY800 spectrometer equipped with two premonochromators, a spectrograph, and a CCD camera (Wright Instruments) as the detector. The 514.5-nm line of an Ar^+ ion laser (Coherent, Model Innova 90-5) afforded the means of excitation. Spectra were recorded with a resolution of 1.5 cm^{-1}.

DOI: 10.1021/ic501825r
Inorg. Chem. 2015, 54, 1240−1253

■ ASSOCIATED CONTENT

Supporting Information

Single-crystal crystallographic data (NP-SiS_2, HP1-SiS_2, HP2-SiS_2, and HP3-SiS_2), Diamond2 views on four GeS_2 phases, as well as experimental and theoretical Raman spectra. This material is available free of charge via the Internet at http://pubs.acs.org.

■ AUTHOR INFORMATION

Corresponding Authors

*E-mail: Juergen.Evers@cup.uni-muenchen.de (J. Evers).
*E-mail: hansgeorg.schnoeckel@kit.edu.de (H. Schnöckel).

Author Contributions

The manuscript was written through contributions of all authors. All authors have given approval to the final version of the manuscript.

Notes

The authors declare no competing financial interest.

■ ACKNOWLEDGMENTS

The authors thank Prof. Dr. C. Bräuchle and Prof. Dr. T. M. Klapötke (both of Ludwig−Maximilian University, Munich, Germany) and Prof. U. Müller (University of Marburg) for his encouraging support in deriving the Bärnighausen tree, and Prof. Dr. P. Kroll (University of Texas, Arlington) for critical discussions regarding the very high pressure phases of SiS_2. Computational support from Prof. Dr. C. Röhr (University of Freiburg), Dr. G. Eickerling (University of Augsburg), and Dr. M. Allalen (Leibniz-Rechenzentrum (LRZ) of the Bavarian Academy of Science, Garching) is gratefully acknowledged.

■ DEDICATION

This paper is dedicated to Professor Hartmut Bärnighausen, in recognition of his outstanding contributions to solid-state chemistry.

■ REFERENCES

(1) (a) Schnöckel, H.; Köppe, R. *J. Am. Chem. Soc.* **1989**, *111*, 4583−4586. (b) Schnöckel, H. *Angew. Chem.* **1978**, *90*, 638−639. (c) Schnöckel, H. *Angew. Chem., Int. Ed.* **1978**, *17*, 616−617.

(2) (a) Mück, L.; Lattanzi, V.; Thorwirth, S.; McCarthy, M. C.; Gauss, J. *Angew. Chem.* **2012**, *12*, 3755−3758. (b) Mück, L.; Lattanzi, V.; Thorwirth, S.; McCarthy, M. C.; Gauss, J. *Angew. Chem., Int. Ed.* **2012**, *51*, 3695−3698.

(3) Aoki, H.; Syono, Y.; Hemley, R. J. *Physics Meets Mineralogy; Condensed Matter Physics in the Geosciences*; Cambridge University Press: Cambridge, U.K., 2008; p 173.

(4) Villars, P.; Clavert, L. D. *Pearson's Handbook of Crystallographic Data for Intermetallic Phases*, Second Edition, Vol. *4*; ASM International: Materials Park, OH, 1996; pp 4759−4764.

(5) Stishov, S. M.; Popova, S. V. *Geokhimia* **1961**, *10*, 837−839.

(6) Aoki, H.; Syono, Y.; Hemley, R. J. *Physics Meets Mineralogy; Condensed Matter Physics in the Geosciences*; Cambridge University Press: Cambridge, U.K., 2008; p 261.

(7) Kuwayama, Y.; Hirose, K.; Sata, N.; Ohishi, Y. *Science* **2005**, *309*, 923−924.

(8) Tsuchiya, T.; Tsuchiya, J. *Proc. Natl. Acad. Sci., U.S.A.* **2011**, *108*, 1252−1255.

(9) Zintl, E.; Loosen, K. *Z. Phys. Chem. (Leipzig)* **1935**, *A174*, 301−311.

(10) Büssem, W.; Fischer, H.; Gruner, E. *Naturwissenschaften* **1935**, *23*, 740.

(11) Weiss, A.; Weiss, A. *Z. Naturforsch.* **1952**, *B 7*, 483−484.

(12) Peters, J.; Krebs, B. *Acta Crystallogr., Sect. B: Struct. Cystallogr. Cryst. Chem.* **1982**, *B38*, 1270−1272.

(13) Troyanov, S. I. *Zh. Neorg. Khim.* **2000**, *45*, 1619−1624.

(14) Silverman, M. S.; Soulen, J. R. *Inorg. Chem.* **1965**, *4*, 129−130.

(15) Prewitt, C. T.; Young, H. S. *Science* **1965**, *149*, 535−537.

(16) Brehler, B. *Naturwissenschaften* **1959**, *46*, 554.

(17) Guseva, T. A.; Burdina, K. P.; Semenenko, K. N. *Khimiya* **1991**, *32*, 85−90.

(18) Chapman, K. W.; Chupas, P. J.; Kepert, C. J. *J. Am. Chem. Soc.* **2005**, *127*, 15630−15636.

(19) Goodwin, A. L.; Kepert, C. J. *Phys. Rev. B* **2005**, *71*, 140301−14304.

(20) Hibble, S. J.; Hannon, A. C.; Cheyne, S. M. *Inorg. Chem.* **2003**, *42*, 4724−4730.

(21) (a) Evers, J.; Beck, W.; Göbel, M.; Jakob, S.; Mayer, P.; Oehlinger, G.; Rotter, M.; Klapötke, T. M. *Angew. Chem.* **2010**, *122*, 5812−5817. (b) Evers, J.; Beck, W.; Göbel, M.; Jakob, S.; Mayer, P.; Oehlinger, G.; Rotter, M.; Klapötke, T. M. *Angew. Chem., Int. Ed. Engl.* **2010**, *49*, 5677−5682.

(22) Wells, A. F. *Z. Kristallogr. A* **1938**, *100*, 189.

(23) Dittmar, G.; Schäfer, H. *Acta Crystallogr., Sect. B: Struct. Crystallogr. Cryst. Chem.* **1976**, *32*, 1188−1192.

(24) Dittmar, G.; Schäfer, H. *Acta Crystallogr., Sect. B: Struct. Crystallogr. Cryst. Chem.* **1975**, *31*, 2060−2064.

(25) Wang, N.; Horn, E. *Neues Jahrb. Mineral., Monatsh.* **1973**, 413.

(26) (a) MacLachlan, M.; Petrov, S.; Bedard, R. L.; Manners, I.; Ozin, G. A. *Angew. Chem.* **1998**, *110*, 2185−2189. (b) MacLachlan, M.; Petrov, S.; Bedard, R. L.; Manners, I.; Ozin, G. A. *Angew. Chem., Int. Ed.* **1998**, *37*, 2075−2079.

(27) Brandenburg, K. *Visual Crystal Structure Information System, Diamond2*; Crystal Impact GbR: Bonn, Germany, 1999.

(28) Lissner, F.; Schleid, T. *Z. Anorg. Allg. Chem.* **2003**, *629*, 1027−1032.

(29) Schmolke, C.; Lupart, S.; Schnick, W. *Solid State Sci.* **2009**, *11*, 305−309.

(30) Pauling, L. *Die Natur der chemischen Bindung*; Verlag Chemie: Weinheim, Germany, 1964; p 517.

(31) Müller, U. *Anorganische Strukturchemie*; B. G. Teubner: Stuttgart, Germany, 1991; p 58.

(32) Bader, R. F. W. *Atoms in Molecules, A Quantum Theory*; International Series of Monographs in Chemistry, No. *22*; Clarendon Press: Oxford, U.K., 1994.

(33) Schwarz, Kh.; Blaha, P.; Trickey, S. B. *Mol. Phys.* **2010**, *108*, 3147−3166.

(34) Blaha, P.; Schwarz, K.; Madsen, G. D.; Kvasnicka, D. J.; Luitz, J. *WIEN2k, An Augmented Plane Wave Plus Local Orbitals Program for Calculating Crystal Properties*; Vienna University of Technology, Institute of Physical and Theoretical Chemistry: Vienna, Austria, 2012.

(35) Shannon, R. D. *Acta Crystallogr., Sect. A: Cryst. Phys., Diffr., Theor. Gen. Crystallogr.* **1976**, *32*, 751−767.

(36) Neubüser, J.; Wondratschek, H. *Krist. Tech.* **1966**, *1*, 529−543.

(37) Bärnighausen, H. *MATCH* **1980**, *9*, 139.

(38) Meyer, A. Dissertation, Universität Karlsruhe, 1981; Vol. *I*, p 99; Vol. *II*, pp 76, 99.

(39) Müller, U. (University of Marburg). Personal communication with one of the authors (J.E.), Oct. 13 and 17, 2014.

(40) *Symmetry Relations Between Space Groups*, 2nd Edition; Wondratschek, H., Müller, U., Eds.; International Tables For Crystallography, Vol. *A1*; Wiley: Chichester, U.K., 2010.

(41) Müller, U. *Inorganic Structural Chemistry*; Wiley: Chichester, U.K., 2007.

(42) Müller, U. *Symmetry Relationships between Crystal Structures*; Oxford University Press: Cambridge, U.K., 2013.

(43) Müller, U. *Relaciones de simetria entre estructuras cristalinas*; Sintesis: Madrid, Spain, 2013.

(44) Müller, U. *Symmetriebeziehungen zwischen verwandten Kristallstrukturen*; Studienbücher Chemie, Vieweg + Teubner Verlag: Wiesbaden, 2011; pp 206, 328.

DOI: 10.1021/ic501825r
Inorg. Chem. 2015, 54, 1240−1253

(45) Sagel, K. *Tabellen zur Röntgenstrukturanalyse, Anleitungen für die chemische Laboratoriumspraxis*, Vol. *VIII*; Mayer-Kaupp, H., Ed.; Springer−Verlag: Berlin, Göttingen, Heidelberg, 1958; p. 42.
(46) Dovesi, R.; Saunders, V. R.; Roetti, C.; Orlando, R.; Zicovich-Wilson, C. M.; Pascale, F.; Civalleri, B.; Doll, K.; Harrison, N. M.; Bush, I. J.; D'Arco, P.; Llunell, M. *CRYSTAL06, User's Manual*; University of Torino: Torino, Italy, 2006.
(47) Evans, R.; Downs, A. J.; Köppe, R.; Peake, S. C. *J. Phys. Chem. A* **2011**, *115*, 5127−5137.
(48) In the **F**-matrix element $F = f_{SiS} + f_{(SiS/SiS)} + f'_{(SiS/SiS)} + f''_{(SiS/SiS)}$, the different positive bond−bond interaction contributions ($f_{(SiS/SiS)}$, $f'_{(SiS/SiS)}$, and $f''_{(SiS/SiS)}$) represent interacting Si−S bonds with a common Si ($f_{(SiS/SiS)}$) or S ($f'_{(SiS/SiS)}$) atom or Si−S bonds opposite to each other in a Si_2S_2 four-membered ring. See ref 47 and Lesiecki, M. L.; Nibler, J. W. *J. Chem. Phys.* **1975**, *63*, 3452−3461.
(49) In the analogous force constant element of $SiCl_4$, $F = f_{SiCl} + 3f_{(SiCl/SiCl)}$, the values of f_{SiCl} and $f_{(SiCl/SiCl)}$ were determined to be 3.75 and 0.15 mdyn/Å, respectively. See: Clark, R. J. H.; Rippon, D. M. *J. Mol. Spectrosc.* **1972**, *44*, 479−503.
(50) (a) Evers, J. *J. Solid State Chem.* **1978**, *24*, 199−207. (b) Evers, J. *J. Solid State Chem.* **1979**, *28*, 369−377. (c) Evers, J. *J. Solid State Chem.* **1980**, *32*, 77−86.
(51) Evers, J. *Habilitationsschrift*; Fachbereich Chemie und Pharmacie, Ludwig-Maximilian University: Munich, Germany, 1981; pp 26−32.
(52) Louer, D.; Varagas, J. *J. Appl. Crystallogr.* **1982**, *15*, 542.
(53) Smith, G. S.; Snyder, J. *J. Appl. Crystallogr.* **1979**, *12*, 60.
(54) Pathak, P. D.; Vasavada, N. G. *Acta Crystallogr., Sect. A: Cryst. Phys., Diffr., Theor. Gen. Crystallogr.* **1970**, *A26*, 655−658.
(55) Rodriguez-Carvajal, J. R. FullProf, A Program for Rietveld Refinement and Pattern Matching Analysis. In *Abstracts of the Satellite Meeting on Powder Diffraction of Crystallography*, Chester, U.K., 1990; p 127.
(56) Sheldrick, G. M. *SHELXL-97, Program for Crystal Structure Refinement*; Universität Göttingen: Göttingen, Germany, 1997.
(57) *Xcalibur, Gemini X-ray Diffractometer Systems: User Manual*; Agilent Technologies, Inc.: Oxfordshire, U.K., 2013; p 59.

DOI: 10.1021/ic501825r
Inorg. Chem. 2015, 54, 1240−1253